Mapping Nanoscale Variations in Photochemical Damage of Polymer/Fullerene Solar Cells with Dissipation Imaging

Phillip A. Cox,[†] Dean A. Waldow,[‡] Torin J. Dupper,[†,§] Stephen Jesse,[⊥] and David S. Ginger[†,*]

[†]Department of Chemistry, University of Washington, Seattle, Washington 98195, United States, [‡]Department of Chemistry, Pacific Lutheran University, Tacoma, Washington 98447, United States, and [⊥]Center for Nanophase Materials Sciences, Oak Ridge National Laboratory, Oak Ridge, Tennessee 37831, United States. [§]Present address: Department of Chemistry, Northwestern University, Evanston, Illinois 60208, United States.

ABSTRACT We use frequency-modulated electrostatic force microscopy to track changes in cantilever quality factor (*Q*) as a function of photochemical damage in a model organic photovoltaic system poly-[[4,8-bis[(2-ethylhexyl)oxy]benzo[1,2-*b*:4,5-*b*′]dithiophene-2,6-diyl]-[3-fluoro-2-[(2-ethylhexyl)carbonyl]thieno[3,4-*b*]thiophenediyl]] (PTB7) and 3′*H*-cyclopropa[8,25][5,6]fullerene-C71-D5h(6)-3′-butanoic acid, 3′-phenyl-, methyl ester ($PC_{71}BM$). We correlate local *Q* factor imaging with macroscopic device performance and show that, for this system, changes in cantilever *Q* correlate well with changes in external quantum efficiency and can thus be used to monitor local photochemical damage over the entire functional lifetime of a PTB7:$PC_{71}BM$ solar cell. We explore how *Q* imaging is affected by the choice of cantilever resonance frequency. Finally, we use *Q* imaging to elucidate the differences in the evolution of nanoscale structure in the photochemical damage occurring in PTB7:$PC_{71}BM$ solar cells processed with and without the solvent additive 1,8-diiodooctane (DIO). We show that processing with DIO not only yields a preferable morphology for uniform performance across the surface of the device but also enhances the stability of PTB7:$PC_{71}BM$ solar cells—an effect that can be predicted based on the local *Q* images.

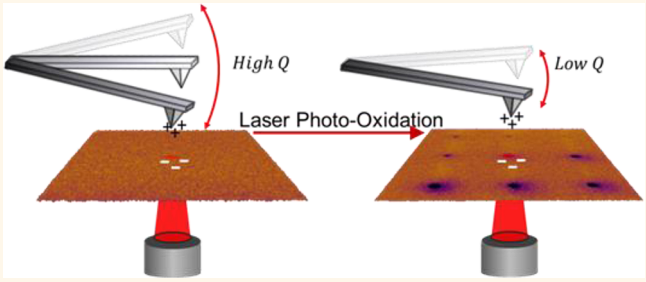

KEYWORDS: atomic force microscopy · organic solar cells · photovoltaics · dissipation imaging · photo-oxidation · photodegradation · PTB7

With champion-cell power conversion efficiencies now crossing the long-sought 10% threshold, organic photovoltaics (OPVs) are gaining more attention as a cost-competitive, renewable energy source.[1,2] For nearly a decade, the major focus of OPV research has been on increasing device efficiencies.[3−5] During this time, comparatively less attention has been given to the stability of these devices.[6−9] While accelerated lifetime testing of encapsulated OPV devices has already been reported to exceed 7 years,[10] the lifetimes of OPVs are still far shorter than the multidecade lifetimes often attributed to traditional inorganic photovoltaics.[6] It thus remains an open challenge to better understand the pathways leading to the degradation of OPVs in order to design longer-lasting materials and device structures.

To date, lifetime studies have yielded important insights into the aging mechanisms of current generations of OPVs.[11−19] For instance, Peters *et al.* tracked power conversion efficiencies of P3HT- and PCDTBT-based solar cells over thousands of hours to understand the "burn-in loss" dominating the degradation time scale.[10] Madsen *et al.* used highly concentrated light of up to 150 suns to accelerate degradation in P3HT films, finding degradation to scale linearly with light intensity.[17] Alem *et al.* have employed conventional techniques such as NMR, XPS, and UV−visible spectroscopy to study oxygen bond formation in the degradation of polymers containing a central benzo[1,2-*b*:4,5-*b*′]dithiophene unit.[18] These studies and others have provided valuable evidence for device degradation mechanisms including the effects of contacts, thermal morphology coarsening, impurities, the role of oxygen and water exposure,[19] and photo-oxidation of active layer materials.[6] While the use of

* Address correspondence to ginger@chem.washington.edu.

Received for review September 20, 2013 and accepted October 7, 2013.

Published online October 08, 2013
10.1021/nn404920t

inverted structures to eliminate reactive metal interfaces,[20−23] cross-linking to reduce morphological coarsening,[24,25] and advances in encapsulation have led to significant increases in practical lifetimes,[26,27] the photochemical stability of the active layers remains an important factor in the long-term lifetime limits that can be achieved.

While most OPV degradation studies so far have relied primarily on measuring bulk device properties as a function of light and oxygen exposure, there is reason to believe that active layer morphology might also play a role in determining photochemical stability. For instance, photocurrent collection maps[28−35] and device models that incorporate energetic disorder[36,37] indicate that, even in fairly efficient devices, the current can be collected predominantly along pathways representing a small fraction of the total film volume. An alternative hypothesis suggests that more ordered regions of a film should exhibit a lower density of tail states, leading to a higher local stability in these regions.[38]

To test such hypotheses, it is important to have tools capable of measuring local variations in electronic properties of OPV films. Scanning Kelvin probe microscopy (SKPM) has also been applied to study photodegradation in model OPV materials,[39,40] though generally without resolving variations due to local composition. In recent studies, our group has used time-resolved electrostatic force microscopy (trEFM)[41] to study photochemical degradation[40,42] in model polymer/polymer donor/acceptor blends and found that device degradation is not uniform across the active area but can depend on active layer morphology. While trEFM is well-suited to degradation studies, its time resolution is insufficient for the study of high-efficiency OPVs under typical solar illumination intensities. We have also developed a next-generation method—fast, free trEFM (FF-trEFM)[43]—but this method is not yet commercially available.

Motivated by the work of Denk and Pohl,[44] who demonstrated that the dissipation of an oscillating atomic force microscope (AFM) cantilever could be used to measure doping-induced variations in sample conductivity in inorganic semiconductors, our goal herein is to show that dissipation mapping using frequency-modulated electrostatic force microscopy (FM-EFM) can provide a sensitive, noncontact probe of photochemically induced changes in the electronic properties of bulk heterojunction organic photovoltaics. In FM-EFM, as implemented on our system (Asylum MFP-3D), the cantilever is lifted to a particular height above the sample (typically ∼10 nm) and kept at constant phase relative to the drive by modulating the frequency of the shake piezo. A positive DC bias is applied to the cantilever while the active layer of the sample is photoexcited. The electrostatic interactions between the tip and the sample lead to a force gradient which changes the cantilever resonance frequency and can be used to image variations in surface potential and capacitive gradient.[45] In addition, *via* long-range Coulomb interactions, the cantilever can lose energy to the motion of charges in the sample,[44,46] resulting in a reduction in cantilever amplitude—even while the frequency feedback is adjusted to keep the cantilever on resonance.

Here, using model blends of PTB7:$PC_{71}BM$,[47] we show that maps of cantilever dissipation measured with FM-EFM are sensitive to photochemical damage in organic semiconductors, and that these maps are dependent on the chosen cantilever resonance frequency. Additionally, we compare dissipation maps between PTB7:$PC_{71}BM$ films with different processing parameters and provide a link between morphology, bulk device performance, and aging behavior in this system.

RESULTS AND DISCUSSION

Figure 1 shows the chemical structures, UV−vis absorption spectra, and photovoltaic device properties for the PTB7:$PC_{71}BM$ blend devices we used in this study. PTB7 absorbs strongly between 600 and 700 nm, while the fullerene absorption contributes more at shorter wavelengths (300−600 nm). We photooxidized the blend films using a 660 nm LED (LEDEngin LZ1-10R200) to preferentially excite the polymer material during degradation. Figure 1B shows UV−vis spectra collected after subjecting the blend films to a range of exposed photon doses from 150 to 900 J/cm^2. Over this dose range, the fullerene contribution to the film absorbance at shorter wavelengths (300−600 nm) remains constant throughout the degradation process. However, the PTB7-dominated absorption at longer wavelengths (600−700 nm) diminishes gradually as a function of photon dose, eventually decreasing to ∼40% of its original absorbance value after an exposed photon dose of 900 J/cm^2, consistent with photobleaching of the PTB7 chromophore upon exposure to 660 nm light in air. Photobleaching leads to a decrease in light absorption and concomitant reduction in exciton generation that can account for some of the decrease in external quantum efficiency (EQE) we observe in the same spectral region shown in Figure 1B. However, the observed reduction in photocurrent *cannot* result solely from decreased light absorption: the decrease in EQE is much larger than the decrease in absorption at the PTB7 absorption maximum (see Supporting Information Figure S1), and we observe a reduction in EQE at all wavelengths despite the lack of change in the absorption of the film in the shorter wavelength region (∼300−600 nm). This behavior would be consistent with decreases in EQE arising from chemical degradation of the film that results in increasing recombination loss (poorer carrier collection), as well as a decrease in light absorption near the polymer peak.

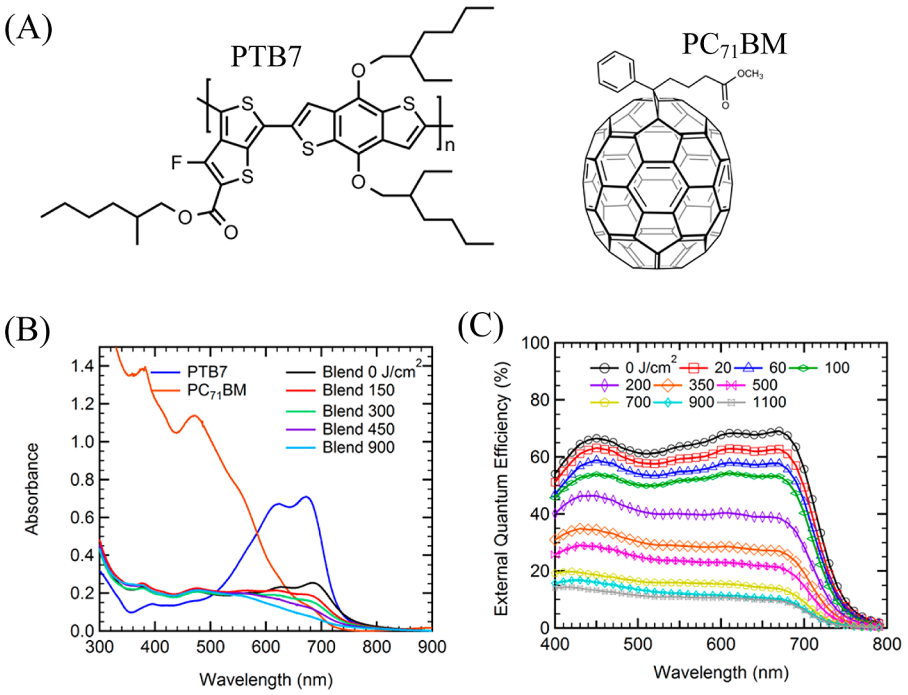

Figure 1. (A) Chemical structures of polymer PTB7 and fullerene $PC_{71}BM$. (B) UV−vis spectra of neat PTB7 polymer and $PC_{71}BM$, as well as the blend film as a function of photon dose. (C) External quantum efficiencies of devices photo-oxidized over photon doses ranging from 0 to 1100 J/cm^2 as indicated in the legend.

In order to explore how photo-oxidation leads to local changes in device performance, we first photo-oxidized a film *in situ* using the focused spot (~1 μm in diameter) from a HeNe laser (intensity 6600 W/m^2) in air. We then purged the sample with dry nitrogen and imaged the same region of the film using FM-EFM under cw illumination, recording topography during the first pass, then cantilever frequency shift ($\Delta\omega$) and cantilever amplitude (A) during a second pass using a cantilever lift height of 10 nm to retrace the topography at a fixed distance.

Figure 2 shows typical data for a 3% DIO PTB7:$PC_{71}BM$ film imaged with FM-EFM. Figure 2A shows a plot of the photon doses that we used at each point, consisting of areas roughly 10 μm apart that were sequentially subjected to increasing photon doses (~20−1200 J/cm^2) in the presence of air. The topography of the film, shown in Figure 2B, appears unchanged by photo-oxidation at these doses. We plot the changes in cantilever dissipation at each position as change in cantilever quality factor (ΔQ) divided by the quality factor (Q). We calculate $\Delta Q/Q$ directly from $\Delta A/A$ (see Supporting Information). In contrast, to the topography, the $\Delta Q/Q$ image in Figure 2C shows clear contrast between the pristine and damaged regions of the film. Figure 2 shows that cantilever Q is very sensitive to local photodegradation: we measure an approximately 1% difference in Q between the fresh and most-degraded areas. In comparison, the relative cantilever frequency exhibits a change of only a few hertz, or about 0.0015%. In general, Q decreases over the degraded areas of the film, though this effect is frequency-dependent (see below). While we have so far assumed these changes in Q result primarily from damage to the active layer, we estimate that even under photoexcitation conditions (carrier densities of ~10^{17}/cm^3) the probe depth of the cantilever would extend through the active layer film. We thus cannot rule out degradation in PEDOT:PSS as contributing to the observed changes in Q. However, as discussed below, the susceptibility of the film to photodamage is sensitive to the use of a solvent additive in the active layer, suggesting that changes in the active layer are the dominant effect.

Cantilever power dissipation is a well-studied phenomenon[44,48−54] but, to our knowledge, has not previously been applied to organic photovoltaics. The quality factor, Q, of a cantilever is inversely proportional to local power dissipation for frequency-modulated techniques:[50,55]

$$P_{tip} = \frac{1}{2}kA^2\omega_0\left[\frac{1}{Q_0} - \frac{1}{Q}\right] \quad (1)$$

In eq 1, k and A are the cantilever spring constant and tip amplitude, ω_0 and Q_0 are the resonance frequency and quality factor measured far from the sample surface, and Q is the quality factor close to the surface. The quality factor of the cantilever is proportional to the tip amplitude:

$$Q = \frac{A}{A_d} \quad (2)$$

This relationship is valid assuming (1) the tip amplitude is measured at the maximum height of the resonance curve,

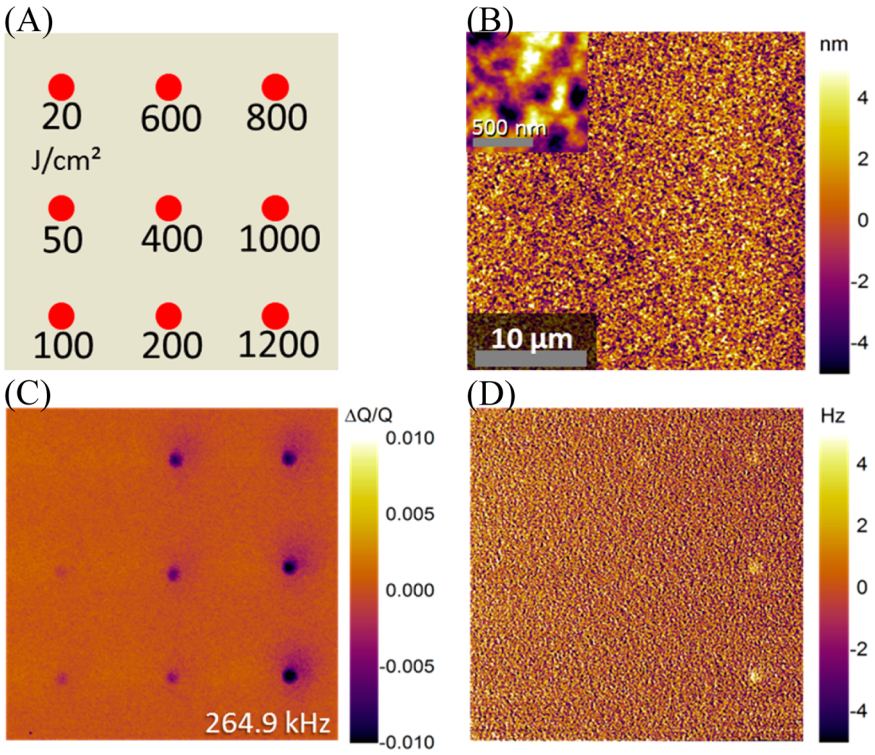

Figure 2. (A) Schematic of the *in situ* photon doses delivered to the sample with a 632.8 nm HeNe laser. (B) Topography (inset 1×1 μm with 500 nm scale bar), (C) $\Delta Q/Q$, and (D) frequency shift measured while imaging a 3% DIO PTB7:$PC_{71}BM$ film photo-oxidized according to the schematic in (A) and imaged with a cantilever driven at 264.9 kHz under 5050 W/m^2 of cw 660 nm light. The scale bar is 10 μm with an overall image length and height of 30 μm.

and (2) the cantilever motion is well-described by a simple linear harmonic oscillator. We chose feedback settings to maintain condition (1) and verified that condition (2) held for our samples by obtaining band excitation[55,56] images conducted at Oak Ridge (Supporting Information Figure S2).

Under these conditions, we can interpret the $\Delta Q/Q$ images presented here as maps of cantilever power dissipation in the sample, mediated by long-range electrostatic interactions. The negative $\Delta Q/Q$ values we observe in Figure 2C are thus consistent with increased electrostatic damping of the cantilever motion over the photo-oxidized regions of the sample. We attribute this increased power dissipation to increased resistive losses associated with charge motion at frequencies near the cantilever resonance frequency, in response to the oscillating electric field of the cantilever.

By creating a grid of increasing photon doses such as that shown in Figure 2C, we are able to observe how the cantilever quality factor evolves over the entire lifetime of the device in a single image. Figure 3 compares the locally measured change in cantilever Q to the change in external quantum efficiency of a bulk device exposed to the same photon dose. We highlight that $\Delta Q/Q$ correlates with EQE during the functional lifetime of the device (see Supporting Information). The correlation between these two properties suggests to us that measuring cantilever Q can be an effective method for tracking nanoscale

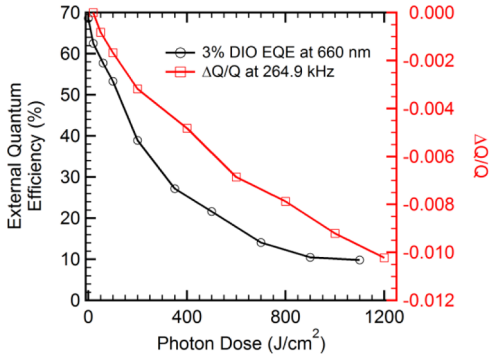

Figure 3. External quantum efficiencies for PTB7:$PC_{71}BM$ devices photo-oxidized in bulk and FM-EFM $\Delta Q/Q$ for a film degraded *in situ* as a function of photon dose.

variations in device performance. This result is particularly valuable because dissipation imaging is readily implemented on commercial instruments without any modification aside from an illumination source. Other methods for measuring local Q, such as band excitation[55,56] or acquiring resonance curves *via* point-by-point frequency sweeps, should allow users with access to a wide range of AFM hardware to probe spatial variation in photo-oxidation in OPV materials by measuring changes in local dissipation. While pcAFM[28−35] can be used to map local changes in photocurrent, pcAFM is a contact mode technique that is poorly suited to *repeated* imaging of soft polymer samples as is needed during degradation studies. Additionally, Q imaging is more sensitive to changes in performance than

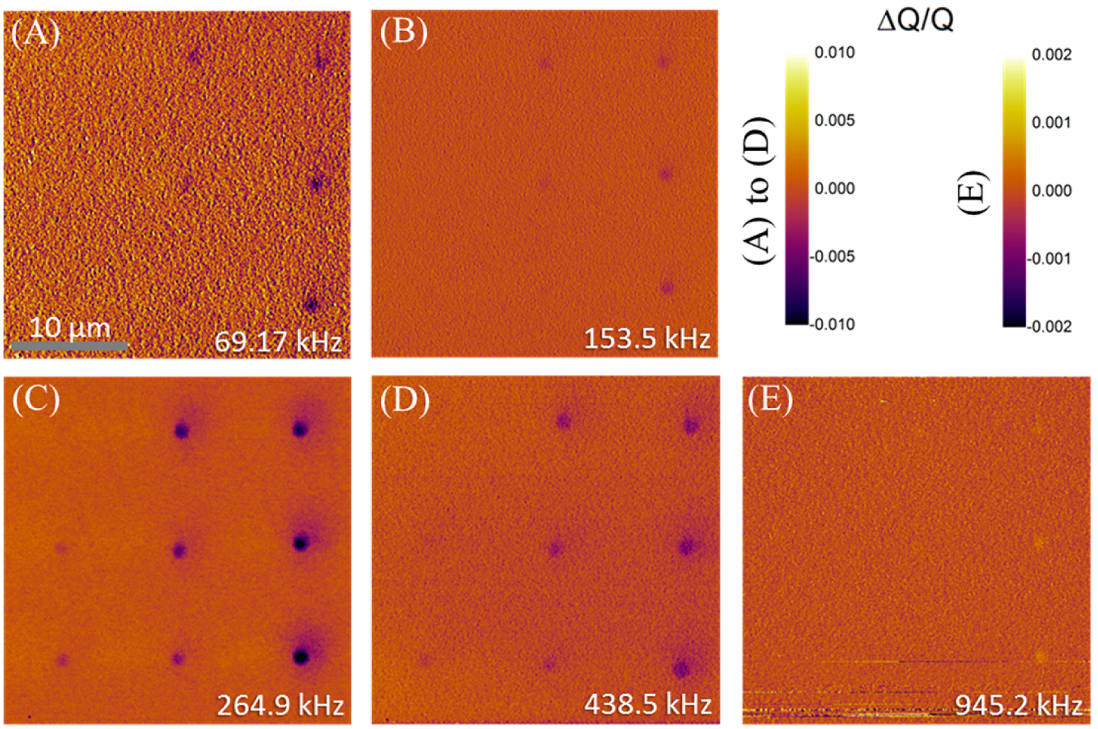

Figure 4. $\Delta Q/Q$ images for (A) 69.17 kHz, (B) 153.5 kHz, (C) 264.9 kHz, (D) 438.5 kHz, and (E) 945.2 kHz cantilevers.

conventional techniques, such as SKPM (Supporting Information Figure S3),[40] which allows us to conduct studies on devices during the initial stages of degradation, before significant changes to surface photovoltage are detectable.

Denk and Pohl have suggested that dissipation imaging is measuring the loss term of the sample dielectric function.[44] This logical proposal would suggest that the choice of cantilever frequency should thus affect the results of a dissipation image. To test this hypothesis, we repeated the FM-EFM experiment depicted in Figure 2 on the same sample using three different cantilevers at five different resonance frequencies (for some cantilevers, we excited both fundamental and higher modes).

Figure 4 shows images of the same 30 μm area of photo-oxidized spots taken at five different cantilever resonance frequencies (69.17, 153.5, 264.9, 438.5, and 945.2 kHz), showing that both the magnitude and sign of the local power dissipation are sensitive functions of the cantilever resonance frequency. Of the frequencies measured, the maximum change in Q occurred with the 264.9 kHz cantilever. Changes in Q were significantly smaller at 153.5 kHz but then increased again at the lowest point of 69.17 kHz. Above 264.9 kHz, the magnitude of the Q changes diminished until at 945.2 kHz Q actually changed sign to show less dissipation in the photo-oxidized areas. In all cases up to a dose of 1200 J/cm^2, the greatest $\Delta Q/Q$ always occurs over the most damaged area (we note that at very high levels of photo-oxidation, beyond those likely to be relevant for device operation, $\Delta Q/Q$ eventually begins to change slope, and even sign, as a function of dosage).

Figure 5 plots $\Delta Q/Q$ as a function of cantilever frequency for three representative photon doses. If FM-EFM probes energy loss processes in the film, then a plot of cantilever power dissipation *versus* frequency should resemble the results of impedance spectroscopy measurements of the imaginary component of the relative permittivity. We note however that while the data in Figure 5 would appear to reflect qualitatively the frequency dependence of the loss term of the local dielectric constant, making such a correlation quantitative would require accounting for the fact that, in changing the frequency of our cantilevers, we also changed the cantilever force constants and free Q values (see Table S1). Within the limited range of frequencies accessible using our current approach, there exists a qualitative similarity between the data in Figure 5 and that published previously by Armbruster and co-workers[57,58] who showed that the imaginary part of the relative permittivity in P3HT:PCBM devices reaches a local maximum in the 10^5 Hz region, a minimum between 10^3 and 10^4 Hz, and then steadily rises as frequency approaches zero. In our PTB7:$PC_{71}BM$ films, we seem to observe a minimum at a higher frequency (around 150 kHz), which could be the result of the differing device mobilities, carrier and trap densities in PTB7 *versus* P3HT films, as well as the absence of the evaporated top metal contacts in our samples.

Finally, given that power dissipation appears to be a powerful way to image variations in photo-oxidative damage to films over time, we applied it to compare the effect of additive processing on the evolution of PTB7:$PC_{71}BM$ blends processed with and without the

solvent additive 1,8-diiodooctane (DIO). DIO is a commonly used solvent additive that has previously been shown to improve morphology and performance (mostly by an increase in fill factor for PTB7:$PC_{71}BM$ devices[47]) of a number of polymer/fullerene bulk heterojunction solar cells.[59] However, how (and if) these changes in morphology are reflected in device aging has not been studied.

We used the same 660 nm excitation LED (operated at a higher intensity of 7500 W/m^2 to accelerate degradation) to degrade large (~2120 μm^2) areas of the device, thereby achieving uniform doses over our imaging fields. As before, we conducted imaging after a thorough (>20 min) purge with dry nitrogen so that damage would not continue during imaging. Figure 6 shows topography and $\Delta Q/Q$ images of PTB7:$PC_{71}BM$ films processed (A) with and (B) without DIO before and after photo-oxidizing to a photon dose of 400 J/cm^2 (see Figure S5 and Figure S6 for $\Delta Q/Q$ images taken at photon doses up to 3000 J/cm^2). The $\Delta Q/Q$ image of the undamaged 3% DIO film is relatively uniform, indicating only minor detectable variations in carrier density/trap density/mobility on the ~10 nm and larger length scale in pristine devices processed with DIO. In contrast, Figure 6B shows the $\Delta Q/Q$ image for a fresh 0% DIO device, where we observe a clear variation in cantilever Q on the same length scale as the obvious variation in surface topography, consistent with compositionally induced variations in electrical dissipation in these less-efficient blends. These local results are in line with the differing device fill factors which indicate that the series resistance/recombination loss is higher in films processed without DIO, as has previously been discussed.[47]

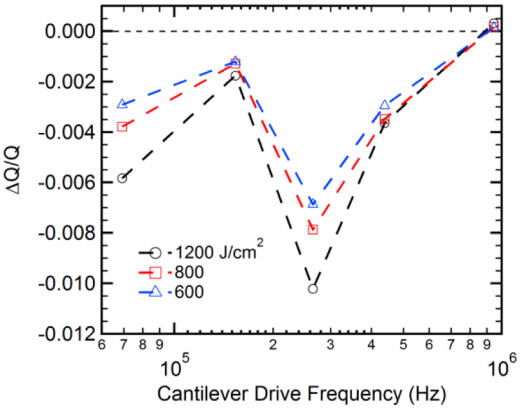

Figure 5. Relationship between $\Delta Q/Q$ and the log of cantilever drive frequency at 1200, 800, and 600 J/cm^2 photon doses.

Interestingly, the use of DIO also affects the way in which the film *degrades*. After a dose of 400 J/cm^2 (which corresponds to about 50% reduction in device performance), the 3% DIO film shows small scale variations in dissipation on ~40 nm length scales, which were nearly invisible prior to photodegradation. On the other hand, the 0% DIO film shows faster degradation, with an overall decrease in the distribution of Q as the areas that started off as low-dissipation are photochemically damaged to a greater extent than the areas that began as lower dissipation. Qualitatively then, the two new films exhibit clear variations in the evolution of the *distribution* of $\Delta Q/Q$ values recorded in each film as the device is further photo-oxidized (see Figure S7). In the case of the 3% DIO film, the *distribution* of $\Delta Q/Q$ is maximized at the same photon dose where the largest shift in cantilever Q was observed in Figure 2C and then tapers off as photon dose approaches 3000 J/cm^2. For 0% DIO films, however, distribution of Q values simply decreases monotonically as a function of photon dose. We believe this difference is

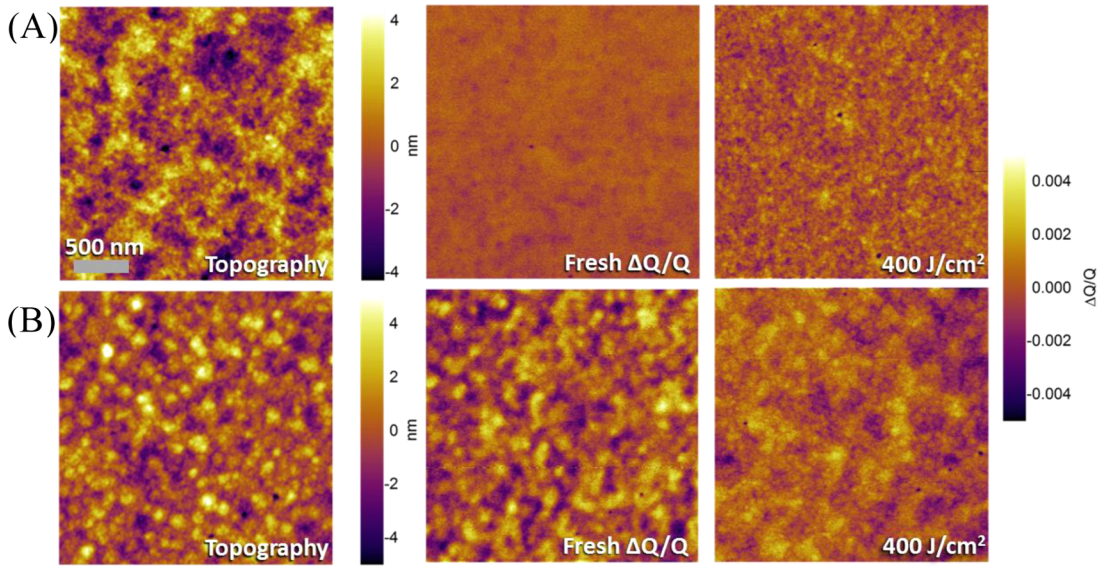

Figure 6. Topography and $\Delta Q/Q$ images for PTB7:$PC_{71}BM$ films processed with (A) 3% and (B) 0% solvent additive 1,8-diiodooctane. Both films were photo-oxidized with a 660 nm LED over a 2120 μm^2 area to an exposed photon dose of 400 J/cm^2. $\Delta Q/Q$ images at additional photon doses can be found in Supporting Information Figure S5 and Figure S6.

due to the decreased stability we see in 0% DIO devices (see Figures S8 and S9). A photon dose of 400 J/cm^2 to a 0% DIO device reduces performance by ~75%, but only ~50% in 3% DIO devices.

CONCLUSIONS

We have used frequency-modulated electrostatic force microscopy to measure changes in cantilever quality factor, or *Q*, as a function of photochemical damage in model PTB7:$PC_{71}BM$ solar cells processed with and without the solvent additive DIO. Our micrometer-spot photo-oxidations show that cantilever power dissipation is initially proportional to photon dose, and as a result, the quality factor of the cantilever declines as a function of damage over the functioning lifetime of the device. By making a direct comparison between our *in situ* dissipation measurements and device performance measurements, we were able to show that local changes in cantilever *Q* correlate well with measured external quantum efficiency changes of PTB7:$PC_{71}BM$ devices. Finally, we compared dissipation maps of PTB7:$PC_{71}BM$ films cast with and without the popular solvent additive DIO. Our results suggest that the morphology achieved when PTB7:$PC_{71}BM$ is processed with DIO leads to more uniform device degradation *via* elimination of hot-spots and bottlenecks throughout the film—consistent with the increased performance of those materials and consistent with the better lifetimes of DIO-processed devices. We expect that dissipation imaging by FM-EFM and band excitation can play an important role in the future design of efficient and stable organic photovoltaics through its ability to map local variations in charge transport and, possibly, to extract information reminiscent of that obtainable with frequency-dependent local impedance spectroscopy.[60]

METHODS

Device Preparation. PTB7:$PC_{71}BM$ devices were made from separate solutions of 25 mg/mL PTB7 (poly[[4,8-bis[(2-ethylhexyl)oxy]benzo[1,2-*b*:4,5-*b*′]dithiophene-2,6-diyl][3-fluoro-2-[(2-ethylhexyl)carbonyl]thieno[3,4-*b*]thiophenediyl]]) (1-Material) and $PC_{71}BM$ (3′*H*-cyclopropa[8,25][5,6]fullerene-C71-D5h(6)-3′-butanoic acid, 3′-phenyl-, methyl ester) (nano-c) dissolved in dichlorobenzene. After being stirred and heated overnight at 60 °C, the solutions were transferred in 1:1.5 proportions by volume of PTB7 to $PC_{71}BM$, where the solvent additive 1,8-diiodooctane was added at 3% by volume just prior to spin-coating. The resultant solution was spin-coated to a final thickness of about 100 nm under nitrogen onto an ITO substrate with a 30 nm layer of PEDOT:PSS (Clevios P VP AI 4083, H.C. Stark Chemicals). Films were dried overnight in vacuum. For bulk device performance measurements, aluminum contacts were evaporated to a final thickness of 80 nm. Aluminum contacts were evaporated after the degradation process. Bulk devices were degraded under ambient room conditions on a homemade photo-oxidation setup using a 5 W 660 nm LED (LEDEngin LZ1-00R200) with an intensity of ~380 W/m^2. The intensity of the LED was measured with a calibrated Si-photodiode (OSI Optoelectronics) and sourcemeter (Keithley 2400).

Device Testing. External quantum efficiencies were measured with a monochromated 450 W xenon lamp (Oriel) and sourcemeter (Keithley 2400) and calculated using a calibrated Si-photodiode (OSI-Optoelectronics). A device mask was used to cover the same area over each device and the photodiode. UV−visible spectra (Agilent 8453) were collected under ambient conditions with either neat PTB7 (25 mg/mL), neat $PC_{71}BM$ (25 mg/mL), or PTB7:$PC_{71}BM$ blend films spin-coated directly onto glass substrates (no ITO or PEDOT:PSS).

Atomic Force Microscopy. AFM measurements were carried out on an Asylum Research MFP-3D BIO atomic force microscope seated on an inverted Nikon Eclipse Ti microscope and Table Stable vibration isolation stage. Silicon cantilevers (BudgetSensor) with conductive Cr/Pt coating (Multi75-G, Tap190-G, and Tap300-G) of three different resonance frequencies (69.17, 153.5, 264.9 kHz) were used. The 69 and 153 kHz cantilevers were operated in the second mode of the cantilever resonance to obtain the images at 438.5 and 945.2 kHz, respectively. All samples were housed in a flow-cell enclosure to control exposure to air or nitrogen. *In situ* photo-oxidations of ~1 μm spot size were performed with a 5 mW HeNe 632.8 nm laser (Research Electro-Optics), while photo-oxidations of ~2120 μm^2 were performed with a 660 nm LED (LEDEngin LZ10R200). Samples were purged in air for 30 min prior to laser exposure and then purged in nitrogen for 30 min before imaging. During imaging, the sample was under constant illumination to generate charge carriers at 5050 W/m^2 using a 660 nm LED (LEDEngin LZ4-00R200). Both the laser and LED intensities were measured in the same manner as the bulk photo-oxidation LED. FM-EFM images were taken with a lift height of 10 nm and tip bias of +10 V. The drive amplitude of the shake piezo during the EFM pass was set to half of the topography pass amplitude. During the EFM pass, the cantilever phase was held at 90° by modulating the drive frequency of the shake piezo. $\Delta Q/Q$ images are flattened to set the fresh areas of the film as a zero-point to demonstrate the difference in amplitude between damaged and undamaged areas. The $\Delta Q/Q$ value at each photon dose is determined by individually masking each degraded area to get amplitude *versus* sample distance and then extracting the mean of a Gaussian fit.

Conflict of Interest: The authors declare no competing financial interest.

Acknowledgment. This work was initially seeded by the National Science Foundation (NSF) DMR-1005504 and completed under NSF DMR-1306079. D.W. acknowledges NSF for research instrumentation (MRI-0619826). Band excitation measurements were conducted at the Center for Nanophase Materials Sciences, which is sponsored at Oak Ridge National Laboratory by the Scientific User Facilities Division, Office of Basic Energy Sciences, U.S. Department of Energy.

Supporting Information Available: Figure S1: Comparison between EQE and absorption loss as a function of photon dose. Figure S2: FM-EFM and band excitation images collected at ORNL. Figures S3 and S4: SKPM and FM-EFM of PTB7:$PC_{71}BM$ film photo-oxidized with laser exceeding 1200 J/cm^2 photon dose. Table S1: Cantilever constants. Figures S5 and S6: Additional LED-photo-oxidized FM-EFM images of PTB7:$PC_{71}BM$ films processed with and without DIO for photon doses ranging from 0 to 3000 J/cm^2. Figure S7: *Q* distribution comparison for PTB7:$PC_{71}BM$ films processed with and without DIO. Figures S8 and S9: EQE for both 0 and 3% DIO PTB7:$PC_{71}BM$ films photo-oxidized from 0 to 1100 J/cm^2. This material is available free of charge *via* the Internet at http://pubs.acs.org.

REFERENCES AND NOTES

1. Jingbiyou, L. D.; Yoshimura, K.; Kato, T.; Ohya, K.; Moriarty, T.; Emery, K.; Chen, C.-C.; Gao, J.; Li, G.; Yang, Y. A Polymer Tandem Solar Cell with 10.6% Power Conversion Efficiency. *Nat. Commun.* **2013**, 1446.
2. Darling, S. B.; You, F. The Case for Organic Photovoltaics. *RSC Adv.* **2013**, *3*, 17633–17648.

3. Hoppe, H.; Sariciftci, N. S. Organic Solar Cells: An Overview. *J. Mater. Res.* **2004**, *19*, 1924–1945.
4. Thompson, B. C.; Frechet, J. M. J. Organic Photovoltaics—Polymer−Fullerene Composite Solar Cells. *Angew. Chem., Int. Ed.* **2008**, *47*, 58–77.
5. Jorgensen, M.; Norrman, K.; Gevorgyan, S. A.; Tromholt, T.; Andreasen, B.; Krebs, F. C. Stability of Polymer Solar Cells. *Adv. Mater.* **2012**, *24*, 580–612.
6. Jørgensen, M.; Norrman, K.; Krebs, F. C. Stability/Degradation of Polymer Solar Cells. *Sol. Energy Mater. Sol. Cells* **2008**, *92*, 686–714.
7. Lee, J. U.; Jung, J. W.; Jo, J. W.; Jo, W. H. Degradation and Stability of Polymer-Based Solar Cells. *J. Mater. Chem.* **2012**, *22*, 24265–24283.
8. Grossiord, N.; Kroon, J. M.; Andriessen, R.; Blom, P. W. M. Degradation Mechanisms in Organic Photovoltaic Devices. *Org. Electron.* **2012**, *13*, 432–456.
9. Peters, C. H.; Sachs-Quintana, I. T.; Mateker, W. R.; Heumueller, T.; Rivnay, J.; Noriega, R.; Beiley, Z. M.; Hoke, E. T.; Salleo, A.; Mcgehee, M. D. The Mechanism of Burn-In Loss in a High Efficiency Polymer Solar Cell. *Adv. Mater.* **2012**, *24*, 663–668.
10. Peters, C. H.; Sachs-Quintana, I. T.; Kastrop, J. P.; Beaupré, S.; Leclerc, M.; Mcgehee, M. D. High Efficiency Polymer Solar Cells with Long Operating Lifetimes. *Adv. Energy Mater.* **2011**, *1*, 491–494.
11. Khelifi, S.; Decock, K.; Lauwaert, J.; Vrielinck, H.; Spoltore, D.; Piersimoni, F.; Manca, J.; Belghachi, A.; Burgelman, M. Investigation of Defects by Admittance Spectroscopy Measurements in Poly(3-hexylthiophene):(6,6)-Phenyl-C61-Butyric Acid Methyl Ester Organic Solar Cells Degraded under Air Exposure. *J. Appl. Phys.* **2011**, *110*, 094509.
12. Singh, V.; Arora, S.; Bhatnagar, P. K.; Arora, M.; Tandon, R. P. Effects of Aging on the Mobility and Lifetime of Carriers in Organic Bulk Heterojunction Solar Cells. *J. Renewable Sustainable Energy* **2011**, *3*, 063111.
13. Golovnin, I. V.; Bakulin, A. A.; Zapunidy, S. A.; Nechvolodova, E. M.; Paraschuk, D. Y. Dramatic Enhancement of Photooxidation Stability of a Conjugated Polymer in Blends with Organic Acceptor. *Appl. Phys. Lett.* **2008**, *92*, 243311.
14. Krebs, F. C.; Gevorgyan, S. A.; Alstrup, J. A Roll-to-Roll Process to Flexible Polymer Solar Cells: Model Studies, Manufacture and Operational Stability Studies. *J. Mater. Chem.* **2009**, *19*, 5442–5451.
15. Kawano, K.; Pacios, R.; Poplavskyy, D.; Nelson, J.; Bradley, D. D. C.; Durrant, J. R. Degradation of Organic Solar Cells Due to Air Exposure. *Sol. Energy Mater. Sol. Cells* **2006**, *90*, 3520–3530.
16. Aygül, U.; Hintz, H.; Egelhaaf, H.-J.; Distler, A.; Abb, S.; Peisert, H.; Chassé, T. Energy Level Alignment of a P3HT/Fullerene Blend during the Initial Steps of Degradation. *J. Phys. Chem. C* **2013**, *117*, 4992–4998.
17. Madsen, M. V.; Tromholt, T.; Norrman, K.; Krebs, F. C. Concentrated Light for Accelerated Photo Degradation of Polymer Materials. *Adv. Energy Mater.* **2013**, *3*, 424–427.
18. Alem, S.; Wakim, S.; Lu, J.; Robertson, G.; Ding, J.; Tao, Y. Degradation Mechanism of Benzodithiophene-Based Conjugated Polymers When Exposed to Light in Air. *ACS Appl. Mater. Interfaces* **2012**, *4*, 2993–2998.
19. Nikiforov, M. P.; Strzalka, J.; Darling, S. B. Delineation of the Effects of Water and Oxygen on the Degradation of Organic Photovoltaic Devices. *Sol. Energy Mater. Sol. Cells* **2013**, *110*, 36–42.
20. Hau, S. K.; Yip, H. L.; Baek, N. S.; Zou, J. Y.; O'Malley, K.; Jen, A. K. Y. Air-Stable Inverted Flexible Polymer Solar Cells Using Zinc Oxide Nanoparticles as an Electron Selective Layer. *Appl. Phys. Lett.* **2008**, *92*, 253301.
21. Schumann, S.; Da Campo, R.; Illy, B.; Cruickshank, A. C.; Mclachlan, M. A.; Ryan, M. P.; Riley, D. J.; Mccomb, D. W.; Jones, T. S. Inverted Organic Photovoltaic Devices with High Efficiency and Stability Based on Metal Oxide Charge Extraction Layers. *J. Mater. Chem.* **2011**, *21*, 2381–2386.
22. Li, C.-Y.; Wen, T.-C.; Lee, T.-H.; Guo, T.-F.; Huang, J.-C.-A.; Lin, Y.-C.; Hsu, Y.-J. An Inverted Polymer Photovoltaic Cell with Increased Air Stability Obtained by Employing Novel Hole/Electron Collecting Layers. *J. Mater. Chem.* **2009**, *19*, 1643–1647.
23. Sahin, Y.; Alem, S.; De Bettignies, R.; Nunzi, J. M. Development of Air Stable Polymer Solar Cells Using an Inverted Gold on Top Anode Structure. *Thin Solid Films* **2005**, *476*, 340–343.
24. He, D.; Du, X. Y.; Zhang, W.; Xiao, Z.; Ding, L. M. Improving the Stability of P3HT/PC61BM Solar Cells by a Thermal Crosslinker. *J. Mater. Chem. A* **2013**, *1*, 4589–4594.
25. Liu, B.; Png, R. Q.; Zhao, L. H.; Chua, L. L.; Friend, R. H.; Ho, P. K. H. High Internal Quantum Efficiency in Fullerene Solar Cells Based on Crosslinked Polymer Donor Networks. *Nat. Commun.* **2012**, *3*, 1321.
26. Lungenschmied, C.; Dennler, G.; Neugebauer, H.; Sariciftci, S. N.; Glatthaar, M.; Meyer, T.; Meyer, A. Flexible, Long-Lived, Large-Area, Organic Solar Cells. *Sol. Energy Mater. Sol. Cells* **2007**, *91*, 379–384.
27. Krebs, F. C. Encapsulation of Polymer Photovoltaic Prototypes. *Sol. Energy Mater. Sol. Cells* **2006**, *90*, 3633–3643.
28. Pingree, L. S. C.; Reid, O. G.; Ginger, D. S. Imaging the Evolution of Nanoscale Photocurrent Collection and Transport Networks during Annealing of Polythiophene/Fullerene Solar Cells. *Nano Lett.* **2009**, *9*, 2946–2952.
29. Giridharagopal, R.; Ginger, D. S. Characterizing Morphology in Bulk Heterojunction Organic Photovoltaic Systems. *J. Phys. Chem. Lett.* **2010**, *1*, 1160–1169.
30. Rice, A. H.; Giridharagopal, R.; Zheng, S. X.; Ohuchi, F. S.; Ginger, D. S.; Luscombe, C. K. Controlling Vertical Morphology within the Active Layer of Organic Photovoltaics Using Poly(3-hexylthiophene) Nanowires and Phenyl-C61-Butyric Acid Methyl Ester. *ACS Nano* **2011**, *5*, 3132–3140.
31. Dang, X.-D.; Mikhailovsky, A.; Nguyen, T.-Q. Measurement of Nanoscale External Quantum Efficiency of Conjugated Polymer:Fullerene Solar Cells by Photoconductive Atomic Force Microscopy. *Appl. Phys. Lett.* **2010**, *97*, 113303.
32. Dang, X.-D.; Tamayo, A. B.; Seo, J.; Hoven, C. V.; Walker, B.; Nguyen, T.-Q. Nanostructure and Optoelectronic Characterization of Small Molecule Bulk Heterojunction Solar Cells by Photoconductive Atomic Force Microscopy. *Adv. Funct. Mater.* **2010**, *20*, 3314–3321.
33. Coffey, D. C.; Reid, O. G.; Rodovsky, D. B.; Bartholomew, G. P.; Ginger, D. S. Mapping Local Photocurrents in Polymer/Fullerene Solar Cells with Photoconductive Atomic Force Microscopy. *Nano Lett.* **2007**, *7*, 738–744.
34. Xin, H.; Reid, O. G.; Ren, G.; Kim, F. S.; Ginger, D. S.; Jenekhe, S. A. Polymer Nanowire/Fullerene Bulk Heterojunction Solar Cells: How Nanostructure Determines Photovoltaic Properties. *ACS Nano* **2010**, *4*, 1861–1872.
35. Hamadani, B. H.; Gergel-Hackett, N.; Haney, P. M.; Zhitenev, N. B. Imaging of Nanoscale Charge Transport in Bulk Heterojunction Solar Cells. *J. Appl. Phys.* **2011**, *109*, 124501.
36. Van Der Holst, J. J. M.; Uijttewaal, M. A.; Ramachandhran, B.; Coehoorn, R.; Bobbert, P. A.; De Wijs, G. A.; De Groot, R. A. Modeling And Analysis of the Three-Dimensional Current Density in Sandwich-Type Single-Carrier Devices of Disordered Organic Semiconductors. *Phys. Rev. B* **2009**, *79*, 085203.
37. Tessler, N.; Preezant, Y.; Rappaport, N.; Roichman, Y. Charge Transport in Disordered Organic Materials and Its Relevance to Thin-Film Devices: A Tutorial Review. *Adv. Mater.* **2009**, *21*, 2741–2761.
38. Kumar, A.; Hong, Z.; Sista, S.; Yang, Y. The Critical Role of Processing and Morphology in Determining Degradation Rates in Polymer Solar Cells. *Adv. Energy Mater.* **2011**, *1*, 124–131.
39. Sengupta, E.; Domanski, A. L.; Weber, S. A. L.; Untch, M. B.; Butt, H.-J.; Sauermann, T.; Egelhaaf, H. J.; Berger, R. Photoinduced Degradation Studies of Organic Solar Cell Materials Using Kelvin Probe Force and Conductive Scanning Force Microscopy. *J. Phys. Chem. C* **2011**, *115*, 19994–20001.
40. Reid, O. G.; Rayermann, G. E.; Coffey, D. C.; Ginger, D. S. Imaging Local Trap Formation in Conjugated Polymer Solar Cells: A Comparison of Time-Resolved Electrostatic Force Microscopy and Scanning Kelvin Probe Imaging. *J. Phys. Chem. C* **2010**, *114*, 20672–20677.

41. Coffey, D. C.; Ginger, D. S. Time-Resolved Electrostatic Force Microscopy of Polymer Solar Cells. *Nat. Mater.* **2006**, *5*, 735–740.
42. Shao, G.; Rayermann, G. E.; Smith, E. M.; Ginger, D. S. Morphology-Dependent Trap Formation in Bulk Heterojunction Photodiodes. *J. Phys. Chem. B* **2013**, *117*, 4654–4660.
43. Giridharagopal, R.; Rayermann, G. E.; Shao, G.; Moore, D. T.; Reid, O. G.; Tillack, A. F.; Masiello, D. J.; Ginger, D. S. Submicrosecond Time Resolution Atomic Force Microscopy for Probing Nanoscale Dynamics. *Nano Lett.* **2012**, *12*, 893–898.
44. Denk, W.; Pohl, D. W. Local Electrical Dissipation Imaged by Scanning Force Microscopy. *Appl. Phys. Lett.* **1991**, *59*, 2171–2173.
45. Silveira, W.; Marohn, J. Microscopic View of Charge Injection in an Organic Semiconductor. *Phys. Rev. Lett.* **2004**, *93*, 116104.
46. Lekkala, S.; Hoepker, N.; Marohn, J. A.; Loring, R. F. Charge Carrier Dynamics and Interactions in Electric Force Microscopy. *J. Chem. Phys.* **2012**, *137*, 124701.
47. Liang, Y.; Xu, Z.; Xia, J.; Tsai, S. T.; Wu, Y.; Li, G.; Ray, C.; Yu, L. For the Bright Future—Bulk Heterojunction Polymer Solar Cells with Power Conversion Efficiency of 7.4%. *Adv. Mater.* **2010**, *22*, E135–E138.
48. Stowe, T. D.; Kenny, T. W.; Thomson, D. J.; Rugar, D. Silicon Dopant Imaging by Dissipation Force Microscopy. *Appl. Phys. Lett.* **1999**, *75*, 2785–2787.
49. Anczykowski, B.; Gotsmann, B.; Fuchs, H.; Cleveland, J. P.; Elings, V. B. How To Measure Energy Dissipation in Dynamic Mode Atomic Force Microscopy. *Appl. Surf. Sci.* **1998**, *140*, 376–382.
50. Cleveland, J. P.; Anczykowski, B.; Schmid, A. E.; Elings, V. B. Energy Dissipation in Tapping-Mode Atomic Force Microscopy. *Appl. Phys. Lett.* **1998**, *72*, 2613–2615.
51. Dedkov, G. V. On the Dissipation of Mechanical Energy in a Noncontact Dynamic Mode of a Scanning Probe Microscope under Vacuum. *Phys. Solid State* **2006**, *48*, 747–752.
52. Gannepalli, A.; Yablon, D. G.; Tsou, A. H.; Proksch, R. Mapping Nanoscale Elasticity and Dissipation Using Dual Frequency Contact Resonance AFM. *Nanotechnology* **2011**, *22*, 355705.
53. Kareem, A. U.; Solares, S. D. Characterization of Surface Stiffness and Probe-Sample Dissipation Using the Band Excitation Method of Atomic Force Microscopy: A Numerical Analysis. *Nanotechnology* **2012**, *23*, 015706.
54. Proksch, R.; Kalinin, S. V. Energy Dissipation Measurements in Frequency-Modulated Scanning Probe Microscopy. *Nanotechnology* **2010**, *21*, 455705.
55. Jesse, S.; Kalinin, S. V.; Proksch, R.; Baddorf, A. P.; Rodriguez, B. J. The Band Excitation Method in Scanning Probe Microscopy for Rapid Mapping of Energy Dissipation on the Nanoscale. *Nanotechnology* **2007**, *18*, 435503.
56. Jesse, S.; Kalinin, S. V. Band Excitation in Scanning Probe Microscopy: Sines of Change. *J. Phys. D: Appl. Phys.* **2011**, *44*, 464006.
57. Armbruster, O.; Lungenschmied, C.; Bauer, S. Investigation of Trap States and Mobility in Organic Semiconductor Devices by Dielectric Spectroscopy: Oxygen-Doped P3HT: PCBM Solar Cells. *Phys. Rev. B* **2012**, *86*, 235201.
58. Armbruster, O.; Lungenschmied, C.; Bauer, S. Dielectric Response of Doped Organic Semiconductor Devices: P3HT:PCBM Solar Cells. *Phys. Rev. B* **2011**, *84*, 085208.
59. Lou, S. J.; Szarko, J. M.; Xu, T.; Yu, L.; Marks, T. J.; Chen, L. X. Effects of Additives on the Morphology of Solution Phase Aggregates Formed by Active Layer Components of High-Efficiency Organic Solar Cells. *J. Am. Chem. Soc.* **2011**, *133*, 20661–20663.
60. Lee, W.; Prinz, F. B.; Chen, X.; Nonnenmann, S.; Bonnell, D. A.; O'Hayre, R. P. Nanoscale Impedance and Complex Properties in Energy-Related Systems. *MRS Bull.* **2012**, *37*, 659–667.